Analysis of the high-temperature flexural strength behavior of $B_4C–TaB_2$ eutectic composites produced by in situ spark plasma sintering

Dmytro Demirskyi † (a), and Oleg Vasylkiv (b).

(a) Nanyang Technological University, 50 Nanyang Avenue, 639798 Singapore

(b) National Institute for Materials Science, 1-2-1 Sengen, Tsukuba, Ibaraki 305-0047, Japan

Abstract

In this study, flexural strength measurements and microstructural studies have been combined to evaluate the effect of elevated temperatures on the fracture behavior of $B_4C–TaB_2$ ceramic composites that have a eutectic structure. Mechanical characterization was carried out at 1600 °C, 1800 °C and 2000 °C. The $B_4C–TaB_2$ eutectic composites were prepared in situ using a spark plasma sintering technique. The eutectic composites exhibited strengths of 483±17 MPa and 525±12 MPa at 1600 °C and 1800 °C, respectively, which is higher than the strength of 430±25 MPa measured at room temperature. The flexural strength of the $B_4C–TaB_2$ eutectic composites was 511±16 MPa at 2000 °C (i.e., 0.86 of the melting point of the $B_4C–TaB_2$ eutectic), indicating plastic behavior. Analyses of the high-temperature flexural strength behavior of this non-oxide eutectic are reported.

Keywords: boron carbide; high-temperature strength; eutectic composite; tantalum diboride; spark plasma sintering.

1. Introduction

Eutectics are the multi-phase composites formed during liquid-phase solidification processes. Both ordered and disordered eutectics are prepared by different methods and involve using

† Author to whom correspondence should be addressed, dmytro.demirskyi@ntu.edu.sg

metallic, oxide and non-oxide ceramic systems [1–12]. Unlike other ceramic composite fabrication processes, the synthesis of eutectic composites in situ during melt solidification provides the advantage that the resulting structures are not dependent on the properties of the starting materials such as particle size or shape but are instead related to solidification conditions. Interest in non-oxide eutectic composites comes from the unique hardness, creep resistance and strength of these composites at room and elevated temperatures. These aligned composites exhibit enhanced bonding between phases as a direct result of the in situ growth process. Hence, eutectics of boron carbide with transition metal diborides are receiving special attention due to the high hardness and elevated flexural strength behavior of the B_4C matrix [4–12].

Recent studies by Demirskyi et al. [7–11] revealed that eutectic composites of boron carbide with transition metals in group 5 of the periodic table can be prepared in situ by spark plasma sintering (SPS). This method provides an opportunity to study non-oxide eutectic composite samples large enough for strength characterization measurements, thus overcoming one of the disadvantages of the directional solidification (DS) method [2–6], where specimen size is limited to the order of millimeters in a direction perpendicular to that used for solidification. Initial work on the B_4C–TaB_2 system showed that eutectic composition ceramics with strengths comparable to those of metal diboride can be produced [11].

Furthermore, previous reports on eutectic composites based on boron carbide prepared using the DS and SPS methods [4–6] suggest that flexural strength is quite sensitive to the processing routes, which can result in different room temperature strengths ranging from 190 to 420 MPa. Moreover, at elevated temperatures as high as 1600 °C, the additional increase in strength can be

gained from a positive contribution of plastic deformation to the fracture process by activating, for instance, the fibril pull-out mechanism.

Whether there is a similar variation in flexural strength for other B_4C-based systems is of practical importance. Knowledge of how the flexural strength varies with contribution of plasticity of the matrix phase and diboride fibrils is of theoretical interest. Hence, the present study is an extension of a previous investigation on the B_4C–TaB_2 system [9,11] and focuses on the high-temperature flexural behavior of the B_4C–TaB_2 system. In particular, the strength and plastic behavior of these eutectic composites at 2000 °C is reported for the first time. Furthermore, we provide an analysis of flexural strength behavior of other non-oxide eutectic systems at high temperature and present our interpretation of the deformation behavior of this unique class of composites at temperatures of approximately 0.8 of their melting point.

2. Materials and Methods

B_4C–composites with a eutectic composition of 33 mol.% TaB_2 were prepared in situ using spark plasma sintering from commercially available TaB_2 (d_{av} = 1–5 µm, <0.5 wt.% C, <0.5 wt.% N, <0.7 wt.% O, Lot # T301160, Japan New Metals Co., Ltd., Japan) and B_4C (d_{av} = 1.5–5.0 µm, B_2O_3 < 0.75 wt.%, C-free < 2 wt.%, Sinopharm Chemical Reagent Co., Ltd., Singapore) powders as starting materials (**Fig. 1**). The mixture and consolidation routine is described in depth elsewhere [11]. SPS was performed at 2350 °C with a nominal dwell time of 1 min using a Dr. Sinter Model 1050 (Sumitomo Coal Mining Co. Ltd., Japan) [13–17]. After SPS was completed, samples were cooled under a constant pressure of 10 MPa to 1800 °C at a rate of 150 °C·min^{-1} and a dwell time of 1 min at this temperature; then, cooling to room temperature was continued

at a rate of 150 °C·min^{-1}. SPS was performed in an atmosphere of argon gas maintained at a flow rate of 2 l·min^{-1}.

After SPS consolidation, a flat surface was formed on the specimens using SiC paper, followed by grinding with diamond disks to produce a 0.5-μm finish. Crack-free ceramic bar specimens were selected for flexural strength tests.

Three-point flexural strength tests were performed on type A bars (1.5×2.0×20 mm) using semi-articulated fixtures according to ASTM Method C1161-11. Electric discharge machining was used to cut specimens with diameter of 30 mm from the bars. Lateral surfaces on the bars were ground and polished using diamond paste to produce a 1-μm surface finish. The three-point flexural strength tests were conducted using Shimadzu AG-X plus (Shimadzu, Japan) equipped with a specially designed high-temperature enclosure (NEMS, Japan) housing W heating elements and capable of temperatures up to 2000 °C. **Figure 2** shows the details of the high-temperature strength apparatus available at NIMS. The temperature inside the hot-zone was controlled by two thermocouples and an IR pyrometer. The pyrometer was used to control of temperatures above 1800 °C.

The vacuum space was pumped to 4·10^{-3} Pa and backfilled with high-purity argon at least 3 times for the elevated temperature tests. A protective atmosphere was maintained by flowing ultra-high purity argon through an internal enclosure.

For the high-temperature flexural strength tests, the following heating schedule was used: heating from room temperature to 200 °C over 10 minutes, and from 200 °C to the testing temperature at a rate of 18 °C·min^{-1}. A dwell time of 5 min at the testing temperature was employed prior to flexural test. After testing, cooling from the testing temperature to room temperature was performed at a rate of 20 °C·min^{-1}. For the linear portion of the load-

displacement curve, we evaluated the elastic modulus (*Ef*) using the procedure described in [11,17].

A span of 16 mm was used during flexural tests. Measurements were performed using a loading speed of 0.5 $mm \cdot min^{-1}$. Three to four samples were tested at each temperature. Microstructural observations and analyses were carried out on polished sections using an SU 8000 cold-emission FE-SEM (Hitachi, Japan). X-ray diffraction (XRD) analysis (Rigaku RINT 2500 HLR, Japan) using Cu Kα radiation was performed on fractured specimens after the high-temperature flexural tests to identify crystalline phases.

3. Results and Discussion

The bulk densities of the spark plasma sintered specimens were 5.01±0.01 g/cm^3. The resulting relative density of the specimens was greater than 99%. This is consistent with data from our previous study [11]. Furthermore, examination of polished surfaces indicated some pores that usually occurred near unreacted tantalum diboride grains 1–5 μm in size were usually located at the edge of the eutectic colonies. The diameter of TaB_2 eutectic inclusions of were 1.3±0.4 μm. Both regular and irregular eutectic structures were observed as in [11] (see **Fig. 1 (c)**).

3.1 Flexural behavior of B_4C–TaB_2 eutectic composites at elevated temperatures

Figure 2 shows loading curves for boron carbide–tantalum diboride eutectic ceramics recorded during the three-point flexural strength tests at different temperatures. Changes in fracture behavior between the room temperature and 1600 °C tests were not observed. For the tests performed at 1800 °C, a change in the testing curve slope was observed, indicating a change in the elastic modulus during testing (**Table 1**). The elastic modulus decreased more rapidly at

2000 °C to 317±13 GPa. At this temperature, all specimens showed a deviation from the 'linear' elastic part of the loading curve, suggesting plastic fracture of the B_4C–TaB_2 eutectic composites.

A change in the elastic modulus during flexural strength tests at elevated temperatures is a natural process reported for metals, alloys, and eutectic or particulate composites [17,18]. In the case of well-studied particulate ZrB_2 ceramics, a similar change in the elastic modulus was attributed to softening of grain boundaries of secondary phases isolated in the triple grain junctions [18]. In the case of B_4C–TaB_2 eutectic composites, previous investigations using SEM, EDX and XRD [9,11] suggested that only B_4C and TaB_2 phases were present in the eutectic composite. Similar to the DS of non-oxide ceramics [4–6], secondary phases were eliminated during eutectic composite processing.

In general, the fracture behavior of the B_4C–TaB_2 eutectic specimens subjected to flexural testing at elevated temperatures was similar to that observed at room temperature (**Fig. 3**) [11]. The distinctive difference in structure was due to the thermal etching in argon and becomes clearer at 1800 °C or at 2000 °C. Some macroscopic cracks were found after testing in all inspected specimens. The presence of cracks was indirectly indicated by 'zig-zag'-like areas on the loading curves (see arrows in **Fig. 3**). These areas underline the intercrystalline (intergranular) fracture mechanism that eutectic composites undergo [5] and are the result of crack initiation and crack propagation that occurs naturally during testing [11]. To confirm that the appearance of zig-zags on the loading curves was not associated with hardware, reference tests of boron carbide monoliths were performed using a 0.5 mm/min loading speed. These loading–force curves were free of steps or zig-zag areas.

Figures 4–6 suggest that cracks formed during the flexural tests were less straight at 1600 °C and 1800 °C and had the same characteristics as microscopic cracks induced during room temperature fracturing and Vickers indentation described in [8–11]. Some crack deflections near the interface between the B_4C matrix and TaB_2 fibrils are clearly visible for the specimens fractured at 1600 °C. For specimens tested at 2000 °C, the fracture analysis suggested that a number of fibril pull-outs occurred, and such fracturing was confirmed from the number of holes with sharp edges. Some TaB_2 fibrils that were pulled out during fracture can be clearly identified at the other side of the crack (**Fig. 6**). These observations suggest that initial fracturing at 2000 °C occurred mainly through the boron carbide matrix, which fractured in a quasi-brittle manner [2]. Furthermore, we did not observe any clear evidence of degradation of the boron carbide matrix during tests at 2000 °C.

Another important observation is that during flexural strength tests at 1600 °C, we observed a small section of brittle-fractured eutectic (see **Fig. 7 (e)**) in the area of the bar that experienced the maximum compressive stress (below the top roller) in specimen #47-III (**Table 1**). In general, it was seen that specimens fractured at 1600 °C had different fractures than observed at room temperature, where fracturing occurred via fibrils: see uneven chipped fibrils shown in **Fig. 7 (a)** or a mixed mechanism where fracturing occurred along different slip planes in the eutectic composite (**Fig. 7 (c)**) [17]. On the tensile side of the bar, and for other specimens tested twice at 1600 °C, we observed fractures identical to those in **Fig. 4** (which was taken in the center of the bar after flexural testing). In the latter case both matrix and fibrils contributed to the fracture process; the fibril pull-out mechanism also contributed to the increase in strength at 1600 °C [3,6,17].

The experimental data collected on flexural strength behavior of B_4C–TaB_2 eutectics (**Table 1**) suggest that the strength increases between room temperature and 1800 °C, followed by a slight decrease at 2000 °C. **Figure 8** illustrates data on the high-temperature strength of B_4C-based and TiB_2-based ceramics reported in [4,6,16,19–22]. It is apparent that despite high strength values of the TiB_2 – B composites, there is an unavoidable decrease in flexural strength at 1800 °C due to an increased contribution of plastic deformation [16]. After SPS consolidation, the TiB_2–B composite had a peculiar structure in which the TiB_2 grains were surrounded by the rigid B_4C matrix. Unlike most studies of the B_4C–TiB_2 system, where composites had a composition similar to the eutectic composition (70/30 mas% B_4C/TiB_2), only 10 wt.% of boron were added before consolidation in study [16]. Hence, the volume occupied by the boron carbide phase after SPS consolidation was significantly lower than that for the eutectic one. A previous study [16] shows the high-temperature limit of TiB_2 ceramics and demonstrates that smart composition engineering can produce particulate composites with good strength up to 1600 °C, but at temperatures equal to or higher than 1800 °C, the high-temperature intergranular fracture is dominant, and the strength essentially is governed by inter-grain bonding. In this respect, previous studies on the flexural strength behavior of eutectic composites indicated that bonding between the matrix and fibrils is different compared to that reported for particulate composites [11,17].

3.2 Phase analysis of bars after flexure at elevated temperatures

Phase analyses performed on the fractured surfaces of bars after flexural tests by XRD (**Fig. 9**) revealed that the main phases were boron carbide ($B_{13}C_2$) and tantalum diboride. For the latter phase, the hexagonal AlB_2 structure is built of hexagonal nets of Ta and triangular nets of pure

boron atoms (**Fig. 9 (c)**). A graphitic network of boron atoms is sandwiched by the metal layers in bulk.

Because the crystal structure of TaB_2 is layered, the physical properties are expected to be highly anisotropic. However, mainly because of the inherent difficulty in growing single crystals of transition metal diborides, in general, due to their high melting points, almost nothing is known how their physical properties vary with crystallographic directions (i.e., internal crystal anisotropy).

We should note that XRD analysis of a bar after a flexural test at room temperature (**Fig. 9 (a)**) showed that the composite is highly anisotropic. Hence, grinding only part of the bar into fine powder allowed us to detect the presence of the boron carbide phase by observing the (021) peak. In this case, the intensity, position and shape of TaB_2 peaks were also changed when compared with the fractured surface of the bar. The d-spacing of the TaB_2 peaks in tested specimens (**Fig. 9 (b)**) were slightly shifted to lower 2θ values at elevated temperatures, which corresponds to a larger d-spacing and higher tensile stress. A change in the d-spacing of the $Zr^{11}B_2$ phase (110) peaks in the ZrB_2–SiC composite by neutron diffraction was evaluated in [23]. The change in d-spacing during heating and cooling exhibited a hysteresis-like behavior. Furthermore, evaluation of the tensile stresses in the $Zr^{11}B_2$ phase suggested the minimum stress was in the (002) direction, while the maximum stress was in the (110) direction.

Nakano et al. suggested that the hardness of TaB_2 single crystals at high-temperature [24] was higher along the [11-20] direction than along the [10-10] direction on the (0001) plane (see the corresponding plane projection in Fig. 9 (c)).

Hunter et al. studied the slip behavior of ZrB_2 [25] and suggested that the low temperature slip systems were found to include *c*-prismatic slip – 1/3 [0001] (-1010) – and an *a*-pyramidal slip –

1/3 [11-20] (-1101), whereas the elevated temperature sample revealed an *a*-basal slip – 1/3 [11-20] (0001).

A study of HfB_2 suggested that the (0001) surface will relax inwards during heating to 2000 °C [26]. This indicates that crystal structures undergo a change at high temperature because of boron desorption. The latter finding agrees with the fact that boron is easy to sublimate at elevated temperatures during single-crystal growth. Thus, intrinsic changes in TaB_2 fibrils can be caused by relaxation of the diboride lattice. Hence, changes in the shape and position of the (100) and (002) XRD peaks shown in **Fig. 9** may serve as a confirmation that both plastic deformation and structural changes are active during the tests conducted at elevated temperatures. At this point it is impossible to confirm that these processes have a direct influence on each other, and reliable data on bulk poly- and single crystals of TaB_2 or B_4C may provide additional insight.

3.3 Analysis of the temperature dependence of flexural strength of non-oxide eutectic composites

To summarize and analyze data on the flexural strength behavior of eutectic and respective monoliths such as TiB_2 or B_4C, one should keep in mind that physical properties of matter such as flexural strength depend on many factors, in particular, on porosity, grain size and impurities. However, for bulk monoliths flexural strength at elevated temperatures may be directly related to the compounds melting point [17,27]. Hence, in comparing temperature dependent properties it would be more correct to keep the ratio of the testing temperature to the meting point (Tmelt) on the absolute scale. Therefore, the results on flexural behavior of some non-oxide compounds (eutectics and bulk monoliths) are summarized in **Figures 10** and **11** as a function of homologous temperature.

The high-temperature behavior of the flexural strength of B_4C–TiB_2 eutectic composites [4] has two extremes: a maximum at 0.65 Tmelt and a clear minimum at 0.4 Tmelt. First, flexural strength decreases due to the anisotropy in the coefficients of thermal expansions (CTE) for the boron carbide matrix. This is followed by an increase in flexural strength, which is attributed to the plastic behavior of boron carbide matrix and titanium diboride inclusions. Finally, at 1600 °C, the different plasticities of TiB_2 and B_4C phases cause a slight decrease in strength.

Data for the flexural strength of boron carbide ceramics are scarce; most noticeably, data for the flexural behavior of B_4C above 1800 °C are yet to be reported [20–22]. For the high-density polycrystalline bulk samples of B_4C at temperatures of 900–1600 °C, the flexural strength was found to have a complex behavior: first, it decreases due to the anisotropy of CTE, which is followed by increase in strength with increasing temperature. This increase was attributed to the increase in the contribution from plastic deformation to the fracture stress above 1500 K [20] and is discussed in depth in [17].

Data on monolithic titanium diboride ceramics suggest a 40% increase in strength can be achieved at 0.45 Tmelt [15,28,29]. An increase in flexural strength was attributed to an increased contribution from plastic deformation to the fracture process. Nevertheless, a further increase in testing temperature over 0.5 Tmelt resulted in a rapid decrease in strength [15]. In this case, TiB_2 monoliths fractured in a quasi-plastic manner and a decrease in flexural strength and elastic modulus was observed. Hence, analysis of data on the flexural strength behavior of monolithic boron carbide and titanium diboride ceramics confirms the initial observations made for B_4C–TiB_2 eutectic composites [4].

Another interesting observation was made in [3] for the LaB_6–ZrB_2 eutectics prepared by DS. These ceramics showed a continuous strength increase with temperature increase (**Fig. 11**). It

was suggested that this behavior was due to increased bonding forces between the matrix and fibers and the development of stress relaxation processes inside ceramic composite. An increase in strength from 630 MPa at room temperature to 950 MPa at 1600 °C was reported. An identical tendency for the increase of flexural strength with temperature was also reported for LaB_6–TiB_2 eutectics [30], although unfortunately, the ceramics bars were too brittle to be tested at room temperature; hence, the data for [30] are not present in **Fig. 11**.

The flexural strength behavior of the B_4C–TaB_2 system seems to follow the trends observed for B_4C–TiB_2 and LaB_6–ZrB_2 eutectic composites. Unfortunately, the flexural strength behavior of the monolithic TaB_2 was never previously reported for such high temperatures. Currently, it is hard to judge whether B_4C–TaB_2 ceramics would experience a decrease in flexural strength at 0.3–0.4 Tmelt of B_4C matrix or would be compensated for by the plasticity of diboride. Hence, additional flexural testing in this peculiar temperature interval is suggested as a topic for upcoming studies. Nevertheless, the primary goal of this study was to evaluate flexural behavior above 1600 °C, and the maximum temperature used for the flexural strength tests in this study is 0.86 of the melting point of the B_4C–TaB_2 system [12]. At such a high temperature, the fracture behavior of polycrystalline specimens of B_4C and TaB_2 phases is expected to be controlled by their plasticity, as was reported in [17] for SiC–NbB_2 eutectics. The SiC–NbB_2 composites showed a decrease of only 10–20% in flexural strength at 1900–2000 °C, only 100–150 °C below their hypothetical melting point [17].

As analyzed in [17] and summarized in a systematic study [27], the plastic fracture should be observed at temperatures between 0.58–0.7 of Tmelt for transition metal carbides and diborides. In addition, according to Kalish et al. [31], fracturing at 1400 °C occurs mainly through an intergranular fracture mechanism. Hence, at temperatures exceeding 0.58 Tmelt, bulk metal

diboride fractures occur by a plastic intergranular mechanism (see data for TiB_2 and TiB_2-B composite in **Fig. 10)**.

Results of the present study suggest that components produced from B_4C–TaB_2 eutectic composites can be used at working temperatures of 1800–2000 °C, where these composites fracture in quasi-brittle manner and possess high strength (525 MPa). Furthermore, the B_4C–TaB_2 system has the second highest melting point for B_4C–MeB_2 composites (Tmelt ~ 2640 K) [12]. The B_4C–HfB_2 ceramics with a slightly higher melting point (~ 2650 K) may show a similar flexural strength behavior. Moreover, the results of [6] for Si-doped B_4C–TiB_2 eutectic composites at 1600 °C suggest that further strength increases are anticipated if appropriate modification of the boron carbide matrix is performed. Alternatively, the further generation of complex B_4C–TaB_2–HfB_2/TiB_2 composites may additionally increase the elevated temperature performance of these ceramic composites due to the formation of interstitial solid solution compounds [15,32,33].

4. Conclusions

B_4C–TaB_2 eutectic composites produced by SPS showed a strength increase from 430±25 MPa at room temperature to 483±17 MPa at 1600 °C. Fractographic analyses suggest that composites fracture in the same manner at room temperature via numerous micro- and macro-cracks that have distinctive crack deflections. An unexpected strengthening of B_4C–TaB_2 eutectic composites occurs at 1800–2000 °C, in the temperature range where most monolithic ceramics experience a decrease in strength. Analysis suggests that the increase in strength is associated with an increased contribution of plasticity from diboride fibrils and the boron carbide matrix, which is consistent with earlier findings on high-temperature behavior non-oxide eutectics.

Acknowledgments

The authors wish to express their appreciation to Dr. Toshiyuki Nishimura (NIMS, Japan) for kindly providing access to and the use of apparatus for measuring strength.

References

[1] R. Elliot, Eutectic Solidification Processing: Crystalline and Glassy Alloys, Butterworths, London, 1983.

[2] F.L. Kennard, R.C. Bradt, V.S. Stubican, Mechanical Properties of the Directionally Solidified MgO-MgAl2O4 Eutectic, *J. Am. Ceram. Soc.,* **59** (1976) 160–163.

[3] I. Bogomol, T. Nishimura, O. Vasylkiv, Y. Sakka, P. Loboda, "The bending strength temperature dependence of the directionally solidified eutectic LaB6–ZrB2 composite," *J. Alloys Compd.*, **509** (2011) 6123–6129.

[4] I. Bogomol, T. Nishimura, O. Vasylkiv, Y. Sakka, P. Loboda, Microstructure and high-temperature strength of B4C–TiB2 composite prepared by a crucibleless zone melting method, *J. Alloys Compd.*, **485** (2009) 677–681.

[5] I. Bogomol, S. Grasso, T. Nishimura, Y. Sakka, P. Loboda, O. Vasylkiv, Hard polycrystalline eutectic composite prepared by spark plasma sintering, *Ceram. Int.*, **38** (2012) 3947–3953.

[6] I. Bogomol, P. Badica, Y.Q. Shen, T. Nishimura, P. Loboda, O. Vasylkiv, Room and high temperature toughening in directionally solidified B_4C-TiB_2 eutectic composites by Si doping, *J. Alloys Comp.,* **570** (2013) 94–99.

[7] D. Demirskyi, Y. Sakka, In Situ Fabrication of B4C–NbB2 Eutectic Composites by Spark–Plasma Sintering, *J. Am. Ceram. Soc.*, **97** (2014) 2376–2378.

[8] D. Demirskyi, Y. Sakka, Fabrication, microstructure and properties of in situ synthesized B4C–NbB2 eutectic composites by spark plasma sintering, *J. Ceram. Soc. Jpn.*, **123** (2015) 33–37.

[9] D. Demirskyi, Y. Sakka, and O. Vasylkiv, Consolidation of B4C–TaB2 eutectic ceramics composites by spark plasma sintering, J. Asian Ceram. Soc., **3** (2015) 369–372.

[10] D. Demirskyi, Y. Sakka, and O. Vasylkiv, Consolidation of B4C–VB2 eutectic ceramics by spark plasma sintering, *J. Ceram. Soc. Jpn.*, **123** (2015) 1051–1054.

[11] D. Demirskyi, Y. Sakka, O. Vasylkiv, High-Strength B4C–TaB2 Eutectic Composites Obtained via in situ by Spark Plasma Sintering, *J. Am. Ceram. Soc.*, **99** (2016) 2436–2441.

[12] S.S. Ordan'yan, A.I. Dmitriev, K.T. Bizhev, E.K. Stepanenko, Interaction in B4C-MeVB2 systems, *Sov. Powder Metall Met. Ceram.*, **26** (1987) 834–836.

[13] D. Demirskyi, Y. Sakka, High-temperature reaction consolidation of TaC–TiB2 ceramic composites by spark-plasma sintering, *J. Eur. Ceram. Soc.*, **35** (2015) 405–410.

[14] D. Demirskyi, Y. Sakka, O. Vasylkiv, High-temperature reactive spark plasma consolidation of TiB2-NbC ceramic composites, *Ceram. Int.*, **41** (2015) 10828–10834.

[15] D. Demirskyi, T. Nishimura, Y. Sakka, O. Vasylkiv, High-strength TiB2–TaC ceramic composites prepared using reactive spark plasma consolidation, *Ceram. Int.*, **42** (2016) 1298–1306.

[16] D. Demirskyi, H. Borodianska, Y. Sakka, O. Vasylkiv, Ultra-high elevated temperature strength of TiB2-based ceramics consolidated by spark plasma sintering, *J. Eur. Ceram. Soc.*, **37** (2017) 393–397.

[17] D. Demirskyi, O. Vasylkiv, Mechanical properties of SiC–NbB2 eutectic composites by in situ spark plasma sintering, *Ceram. Int.*, **42** (2016) 19372–19385.

[18] W.H. Rhodes, E.V. Clougherty, D. Kalish, Research and development of refractory oxidation-resistant diborides Part II, Volume IV: mechanical properties. OH: Air Force Materials Laboratory, Air Force Systems Command: Wright Patterson Air Force Base; 1970 [Technical report AFML-TR-68-190, Part II, Volume IV].

[19] Yu. G. Tkachenko, D. Z. Yurchenko, V. K. Sulzhenko, G. S. Oleinik and V. M. Vereshchaka, Temperature Effect on Bending Strength of Hot-pressed Boron Carbide Materials, *Powder Metall. Met. Ceram*., **46** (2007) 254–260.

[20] G. de With, High Temperature Fracture of Boron Carbide: Experiments and Simple Theoretical Models, *J. Mater. Sci.*, **19** (1984) 457–466.

[21] O. Vasylkiv, D. Demirskyi, H. Borodianska, Y. Sakka, P. Badica, High temperature flexural strength in monolithic boron carbide ceramic obtained from two different raw powders by spark plasma sintering," *J. Ceram. Soc. Jpn.*, **124** (2016) 587–592.

[22] O. Vasylkiv, D. Demirskyi, P. Badica, T. Nishimura, A.I.Y. Tok, Y. Sakka, H. Borodianska, Room and high temperature flexural failure of spark plasma sintered boron carbide, *Ceram. Int.*, **42** (2016) 7001–7013.

[23] J. Watts, G. Hilmas, W.G. Fahrenholtz, D. Brown, B. Clausen, Measurement of thermal residual stresses in ZrB2–SiC composites, *J. Eur. Ceram. Soc.*, **31** (2011) 1811–1820.

[24] K. Nakano, T. Okubo, K. Nakamura, T. Sugimura, High temperature hardness of NbB2 and TaB2 single crystals, *Yogyo Kyokai Shi*, **90** (1982) 285 –289

[25] B. Hunter, X.-X. Yu, N. De Leon, C. Weinberger, W. Fahrenholtz, G. Hilmas, M.L. Weaver, G.B. Thompson, Investigations into the slip behavior of zirconium diboride, *J. Mater. Res.*, **31** (2016) 2749–2756.

[26] W. Hayami, R. Souda, T. Aizawa, T. Tanaka, Structural analysis of the HfB2 (0001) surface by impact-collision ion scattering spectroscopy, *Surf. Sci.*, 415 (1998) 433–437.

[27] P.V. Zubarev, High-temperature strength of the interstitial phases, Metallurgiya, Moscow, 1985 [in Russian].

[28] H.R. Baumgartner, R.A. Steiger, Sintering and properties of titanium diboride made from powder synthesized in a plasma-arc heater, *J. Am. Ceram. Soc.*, **67** (1984) 207–212.

[29] J. Matsushita, T. Suzuki, A. Sano, High Temperature Strength of TiB2 Ceramics, *J. Ceram. Soc. Jpn.*, **101** (1993) 1074–1077.

[30] I. Bogomol, T. Nishimura, O. Vasylkiv, Y. Sakka, P. Loboda, High-temperature strength of directionally reinforced LaB6–TiB2 composite, *J. Alloys Compd.*, **485** (2010) 130–134.

[31] D. Kalish, E.V. Clougherty, K. Kreder, "Strength, Fracture Mode, and Thermal Stress Resistance of HfB2 and ZrB2," *J. Am. Ceram. Soc.*, **52** (1969) 30–36.

[32] P. Schwarzkopf, R. Kieffer, Refractory Hard Metals, Macmillan, New York, 1953.

[33] G.V. Samsonov, L.Ya. Markovskii, A.F. Zhigach, M.G. Valyashko, Boron, Its Compounds and Alloys, Izd. Akad. Nauk UkrSSR, Kiev, 1960 [in Russian].

Tables

Table 1. Evaluation of physical and mechanical properties of B_4C–TaB_2 ceramic composites

Specimen, designation	Temperature, °C	Crosshead rate, $mm \cdot min^{-1}$	Flexural strength, σ, MPa	Elastic modulus, E(f), GPa, (within an error of ±10 GPa)
TB-RT [11]	25	0.5	430	424
47-I	1600	0.5	468	420
47-II	1600	0.5	482	423
47-III	1600	0.5	502	425
45-I	1800	0.5	521	380
45-II	1800	0.5	512	371
45-III	1800	0.5	529	375
45-IV	1800	0.5	540	362
61-I	2000	0.5	519	-*
61-II	2000	0.5	498	-*
61-III	2000	0.5	518	-*

Notes

* B_4C–TaB_2 eutectic composites exhibited plastic behavior (see **Fig. 3**) and the elastic modulus evaluated from the linear slope was 317±13 GPa.

Figure Captions

Fig. 1. SEM images of initial powders (a) B_4C and (b) TaB_2. (c) shows the structure of a eutectic composite formed in situ during SPS. Both regular and irregular eutectic structures can be clearly identified.

Fig. 2. High-temperature strength test apparatus used in the present study for the characterization of the flexural strength of B_4C–TaB_2 eutectic composites. (1) Flexural test machine capable of loads up to 5 kN, (2) high temperature enclosure, (3) controlling unit, (4) thermocouple and (5) IR pyrometer

Fig. 3. Typical loading diagrams of the B_4C–TaB_2 eutectic ceramic composite tested at room temperature and at elevated temperatures by the three-point flexural strength test. Arrows indicate places where non-linear zig-zag-like areas of the load–displacement curves are observed.

Fig. 4. Typical microstructure of the B_4C–TaB_2 eutectic ceramic composite tested at 1600 °C by the three-point flexural strength test. Note the complex nature of the crack propagation that is formed during flexural testing: fibril pull-out, crack deflection and crack bridging mechanisms are active during fracture.

Fig. 5. Fracturing of the B_4C–TaB_2 eutectic ceramic composite tested at 1800 °C by the three-point flexural strength test. Note that markings on the boron carbide matrix are a consequence of thermal etching by the argon gas.

Fig. 6. Cracking and microstructure of the B_4C–TaB_2 eutectic ceramic composite subjected to the three-point flexural strength test at 2000 °C. Note the difference in crack propagations observed at 1600 °C (**Fig. 4**). At 2000 °C, crack opening is easier due to a greater contribution from the plastic deformation to flexure process. The separation between fibrils and the matrix

interface, i.e., intergranular fracture mechanism for particulate composite systems, becomes the main mechanism of fracture.

Fig. 7. Difference in fracture behavior of the B_4C–TaB_2 eutectic ceramic composite fractured by the three-point flexural strength test at room temperature (a–c) and at 1600 °C (d–f). Note that some typical brittle fracture features such as fine cleavage was observed for (e), and are marked by arrows. (e) is taken in the compressive region (i.e., under the top roller), while (d) and (f) are from the tensile region of the bar after the flexural strength test. Dashed lines are used to show the areas of the fiber pull-out.

Fig. 8. Temperature dependence of the flexural strength of B_4C–TaB_2 eutectic and other high-temperature ceramics reported in [4,6,16,19–22]. The dashed line for TiB_2–B composite data is used to illustrate the trend observed in the original study. Note that in some cases, the experimental error bars are smaller than the symbol sizes.

Fig. 9. Phase analysis of the specimens after flexural testing at different temperatures. (a) shows XRD data for initial powders and for the fractured surface of the specimen of after testing at room temperature. Data on a finely ground part of the bars demonstrate the anisotropy of the eutectic ceramic. (b) contains data collected from the flexural surface of bars at 1600 °C and 2000 °C. Note the widening of peaks (100) and (002) identified as TaB_2 with increasing temperature in the tests. (c) shows the crystal structure of TaB_2 and the projection along the [0001] direction.

Fig. 10. Flexural strength behavior of the B_4C–TiB_2 eutectic [4], TiB_2–B composite [16] and B_4C [20–22] and TiB_2 [15,28,29] monoliths as a function of homologous temperature.

Fig. 11. Flexural strength behavior of $B_4C–TaB_2$, $B_4C–TiB_2$, $SiC–NbB_2$ and $LaB_6–ZrB_2$ eutectics as a function of temperature [3,4,17]. Dashed lines in the case of the $B_4C–TiB_2$ and $LaB_6–ZrB_2$ systems highlight trends observed in the original studies.

Figure 1

Click here to download high resolution image

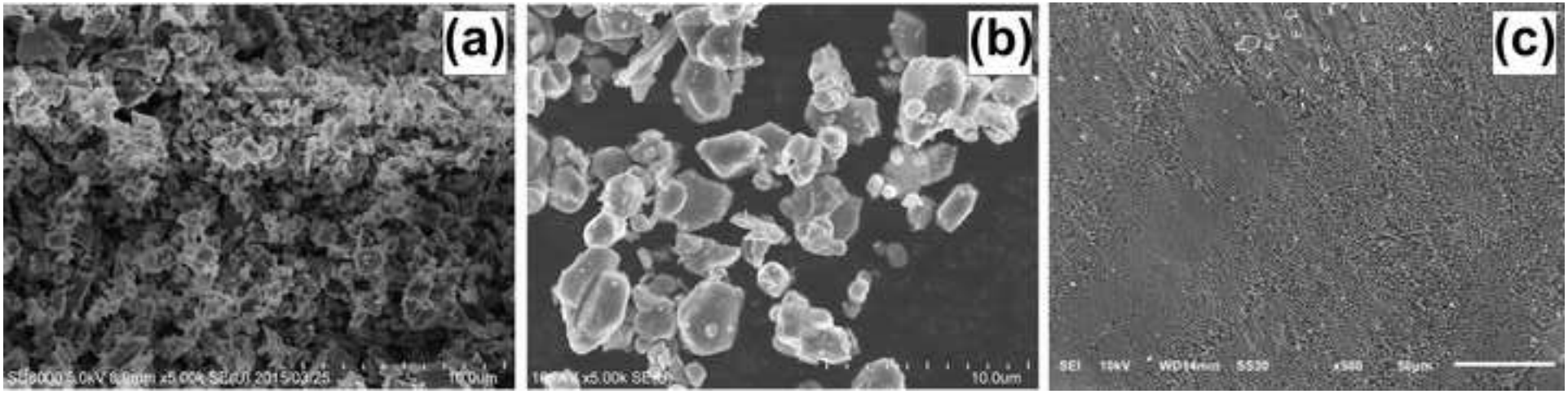

Figure 2

Click here to download high resolution image

Figure 3

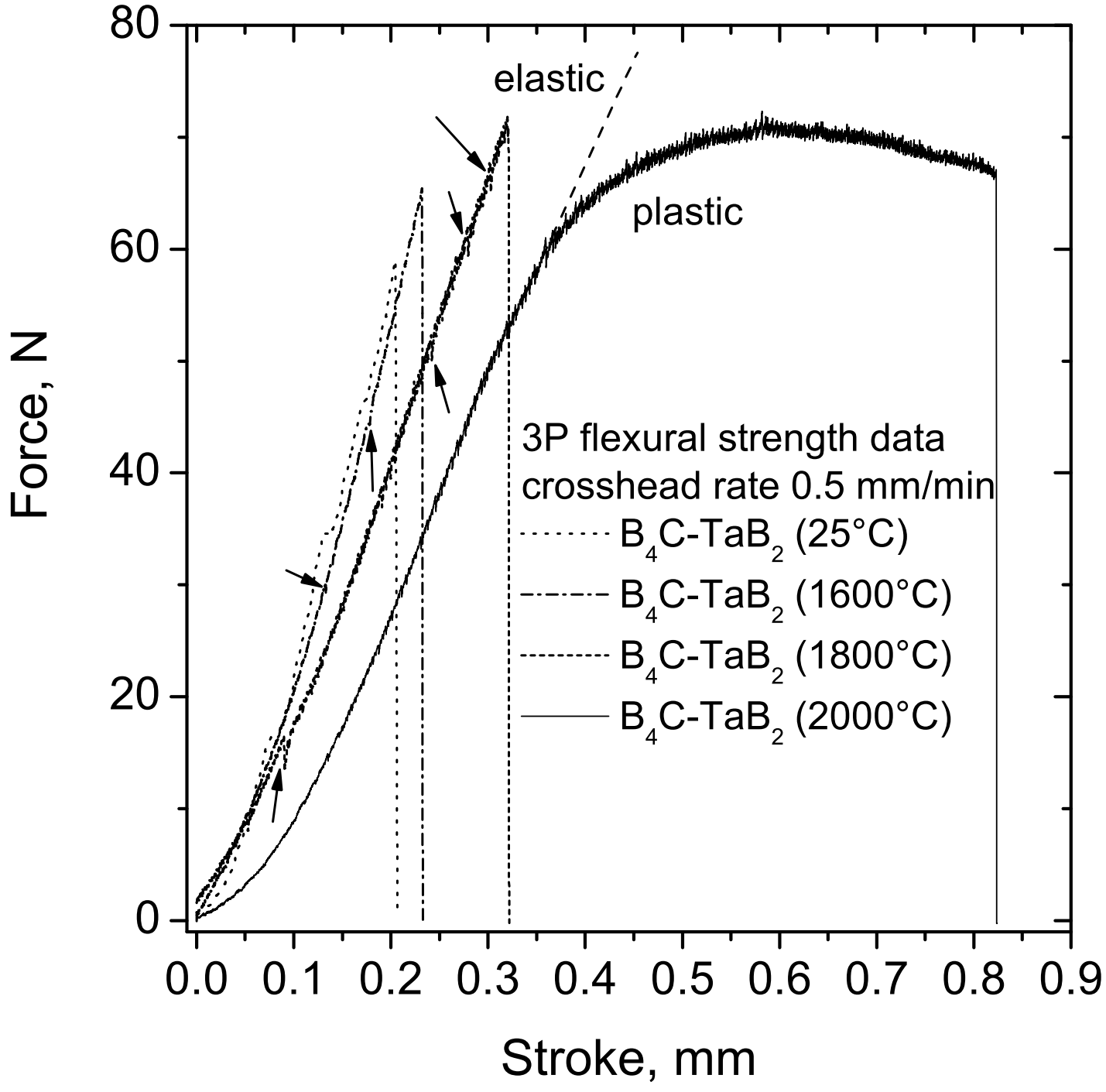
80
60
40
20
0
Force, N
0.0
0.1
0.2
0.3
0.4
0.5
0.6
0.7
0.8
0.9
Stroke, mm
elastic
plastic
3P flexural strength data
crosshead rate 0.5 mm/min
B4C-TaB2 (25°C)
B4C-TaB2 (1600°C)
B4C-TaB2 (1800°C)
B4C-TaB2 (2000°C)

Figure 4

Click here to download high resolution image

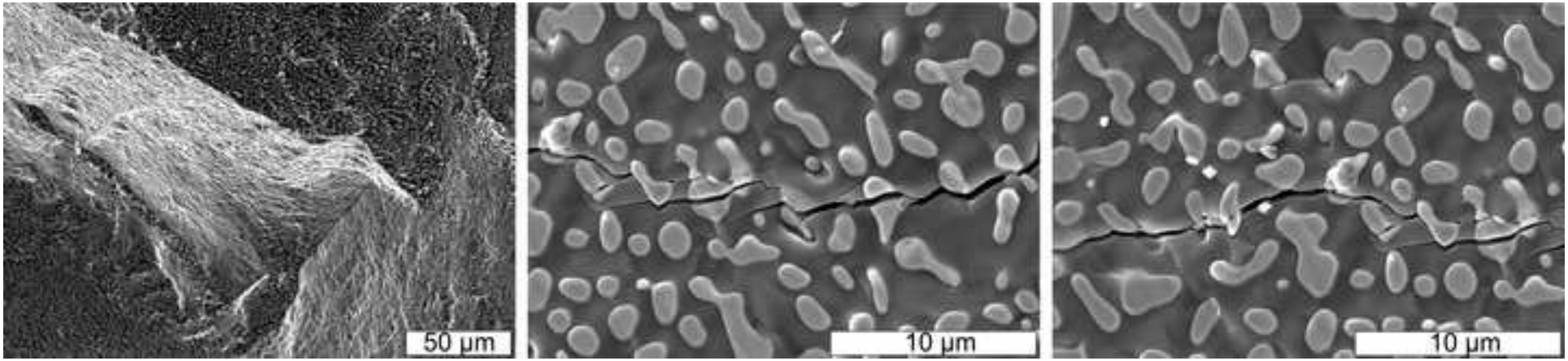

Figure 5

Click here to download high resolution image

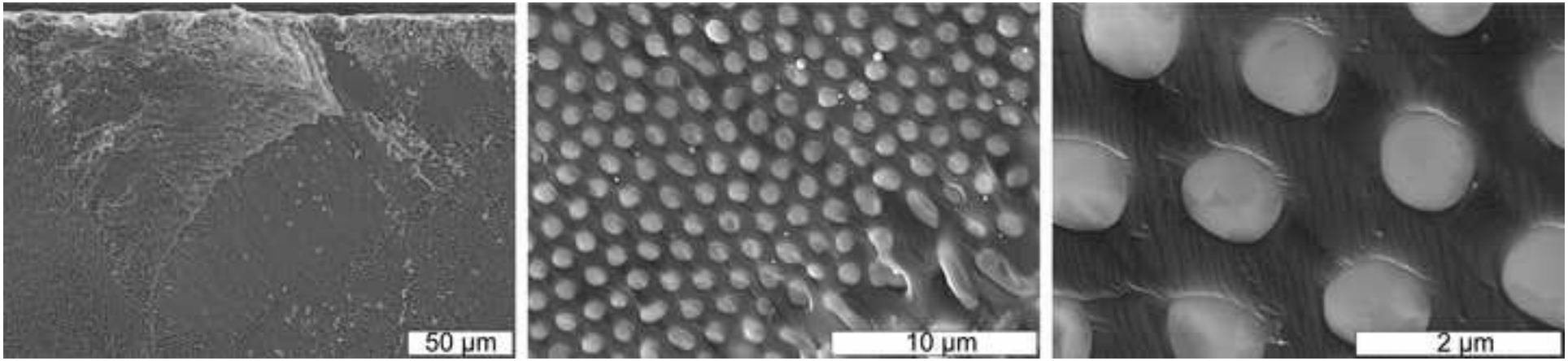

Figure 6

Click here to download high resolution image

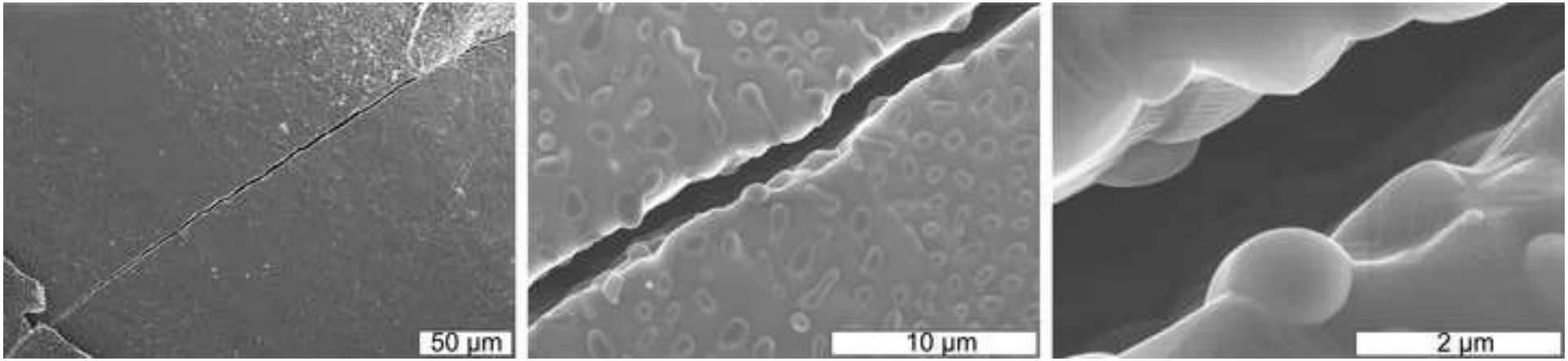

Figure 7

Click here to download high resolution image

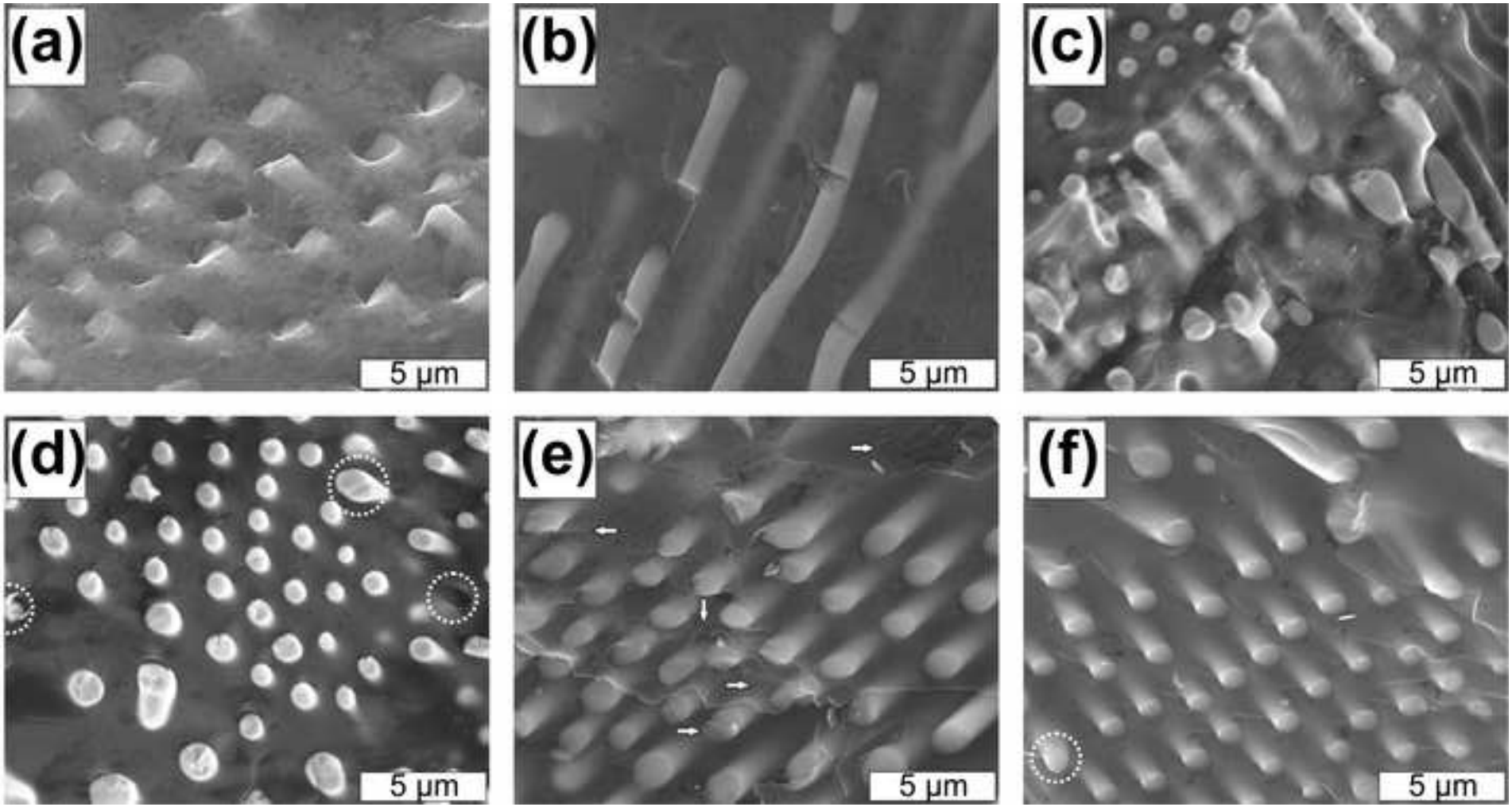

Figure 8

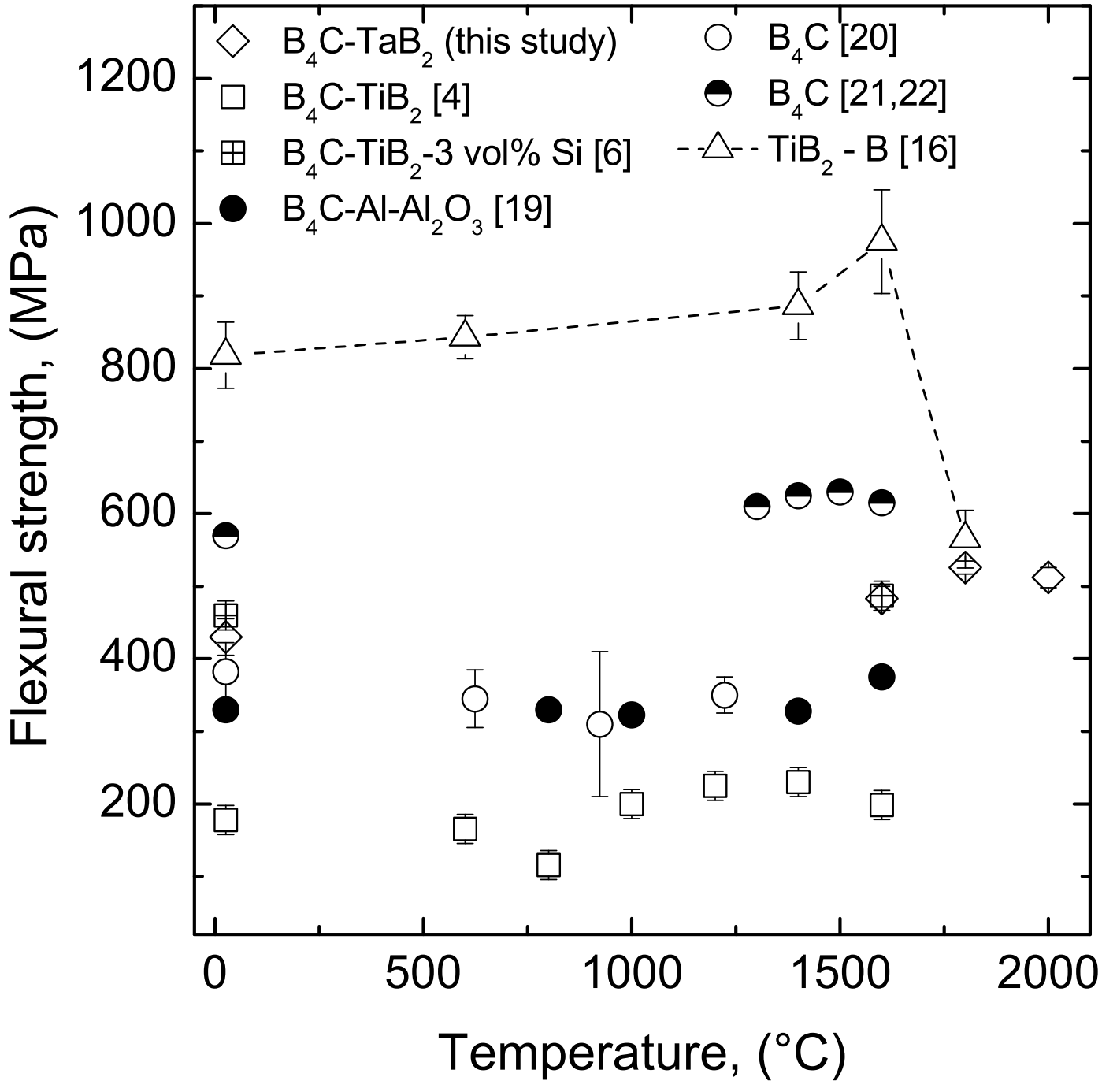
B4C-TaB2 (this study)
B4C-TiB2 [4]
B4C-TiB2-3 vol% Si [6]
B4C-Al-Al2O3 [19]
B4C [20]
B4C [21,22]
TiB2 - B [16]
Flexural strength, (MPa)
Temperature, (°C)
0
500
1000
1500
2000
200
400
600
800
1000
1200

Figure 9ab

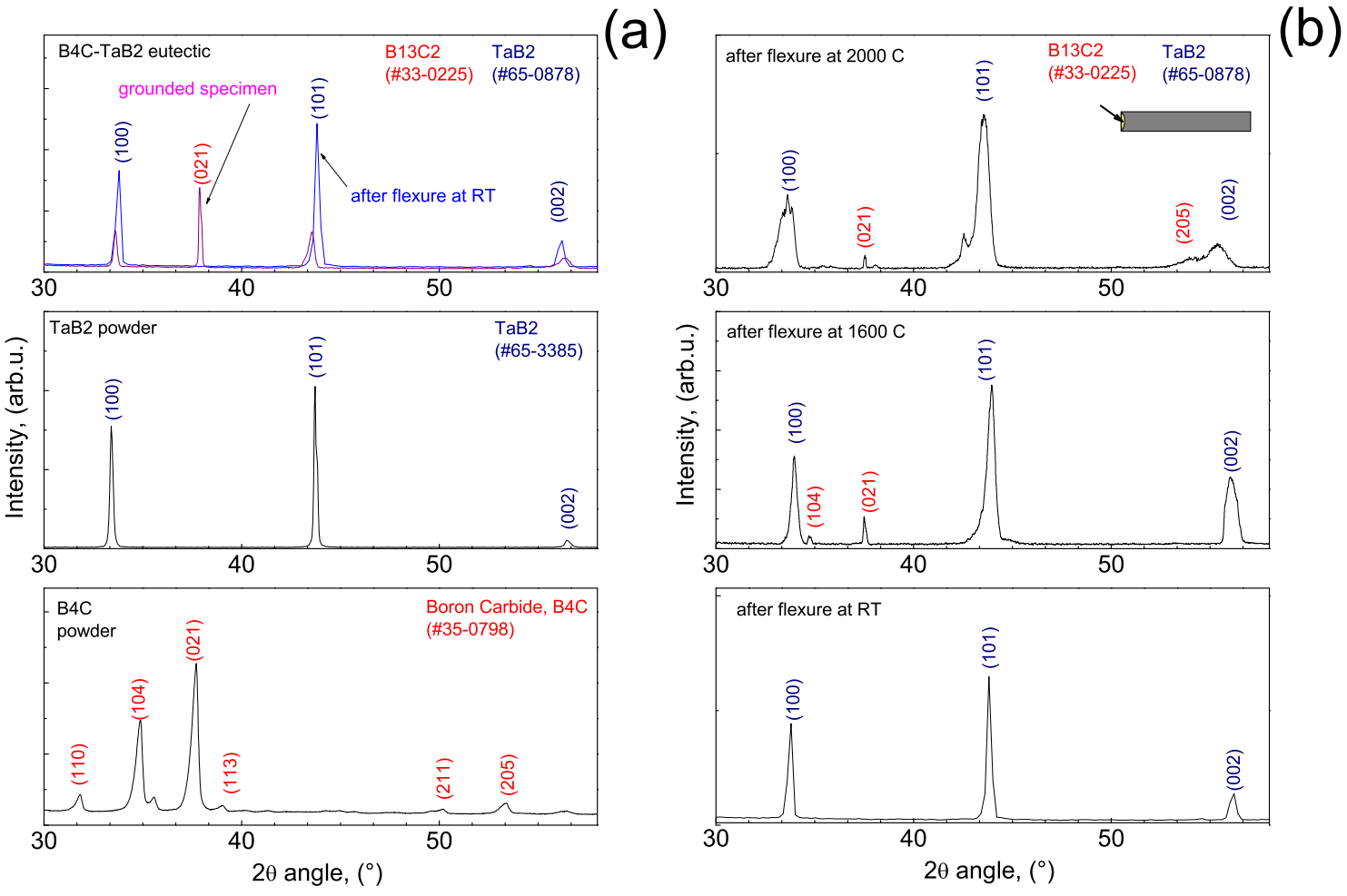
(a)
B4C-TaB2 eutectic
B13C2
(#33-0225)
TaB2
(#65-0878)
grounded specimen
after flexure at RT
(100)
(021)
(101)
(002)
TaB2 powder
TaB2
(#65-3385)
B4C
powder
Boron Carbide, B4C
(#35-0798)
(110)
(104)
(113)
(211)
(205)
Intensity, (arb.u.)
2θ angle, (°)
30
40
50
(b)
after flexure at 2000 C
after flexure at 1600 C
after flexure at RT

Figure 9c

(c)

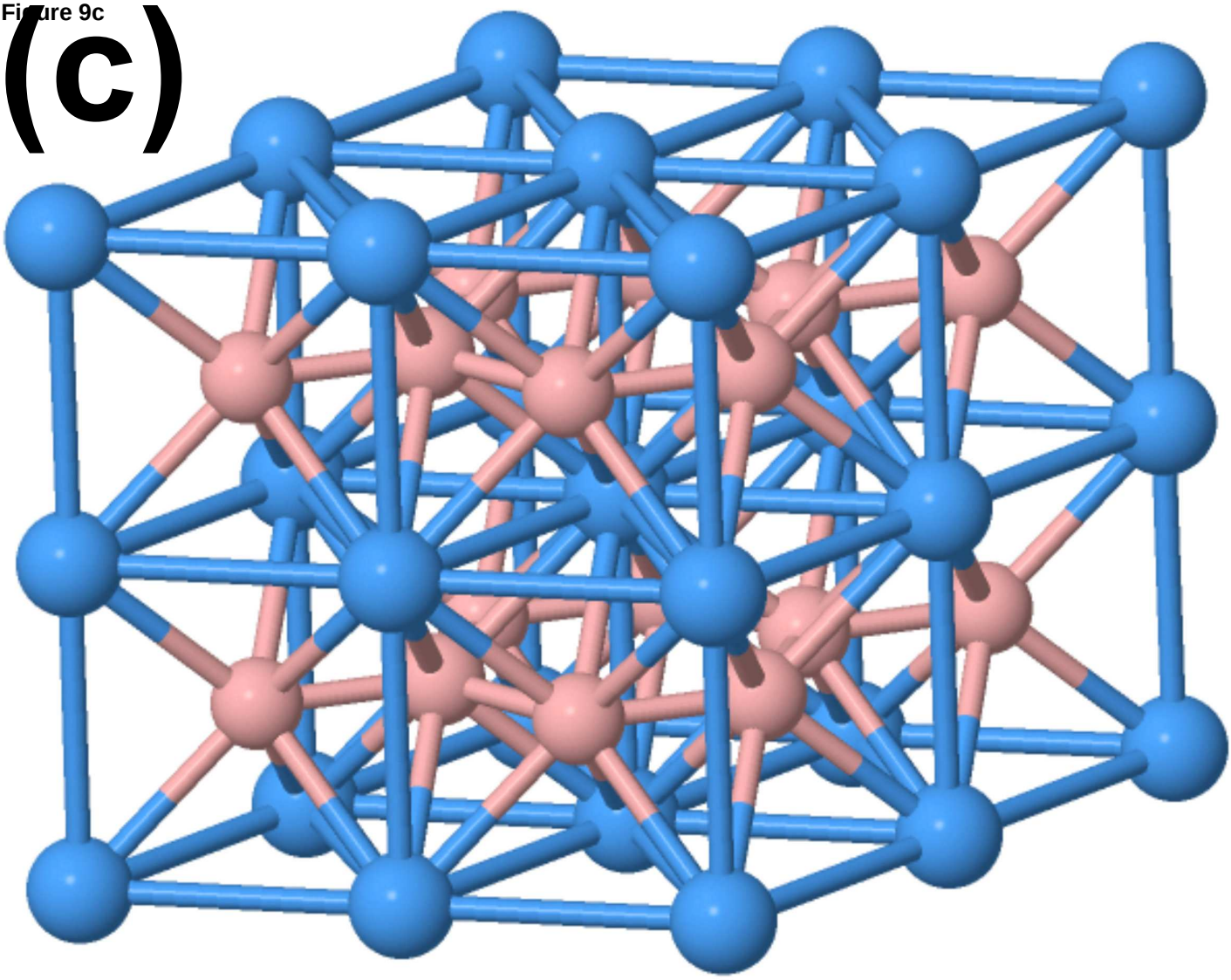

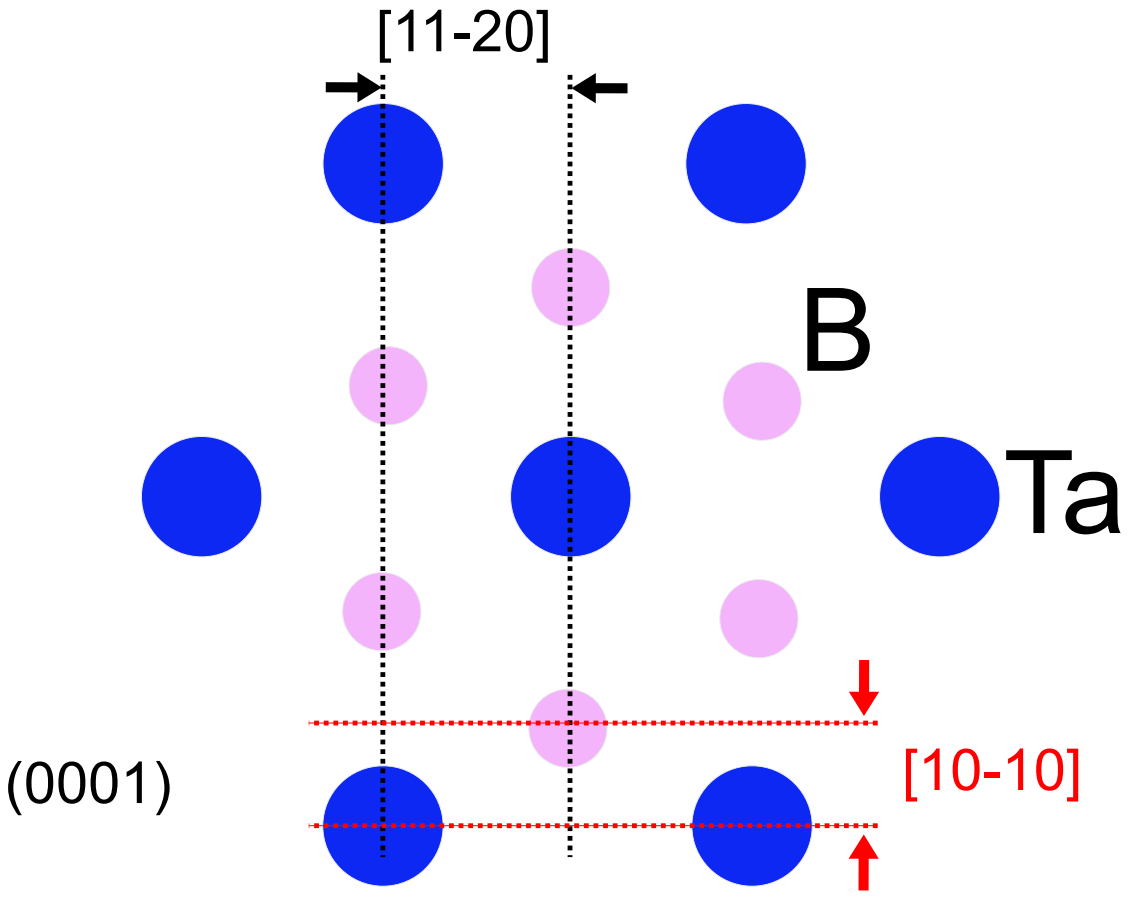

Figure 10

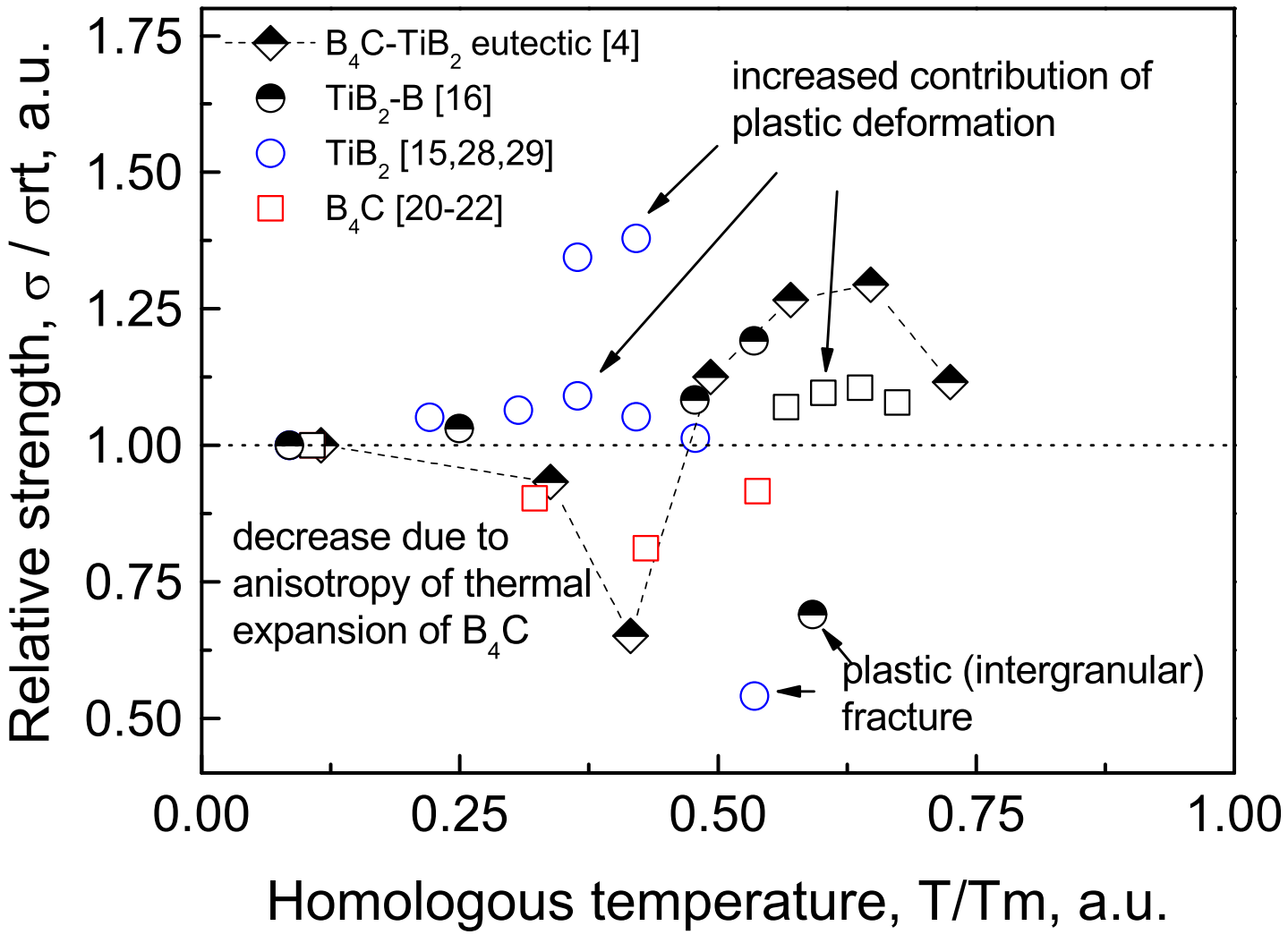
Relative strength, σ / σrt, a.u.
1.75
1.50
1.25
1.00
0.75
0.50
0.00
0.25
0.50
0.75
1.00
Homologous temperature, T/Tm, a.u.
B4C-TiB2 eutectic [4]
TiB2-B [16]
TiB2 [15,28,29]
B4C [20-22]
increased contribution of plastic deformation
decrease due to anisotropy of thermal expansion of B4C
plastic (intergranular) fracture

Figure 11

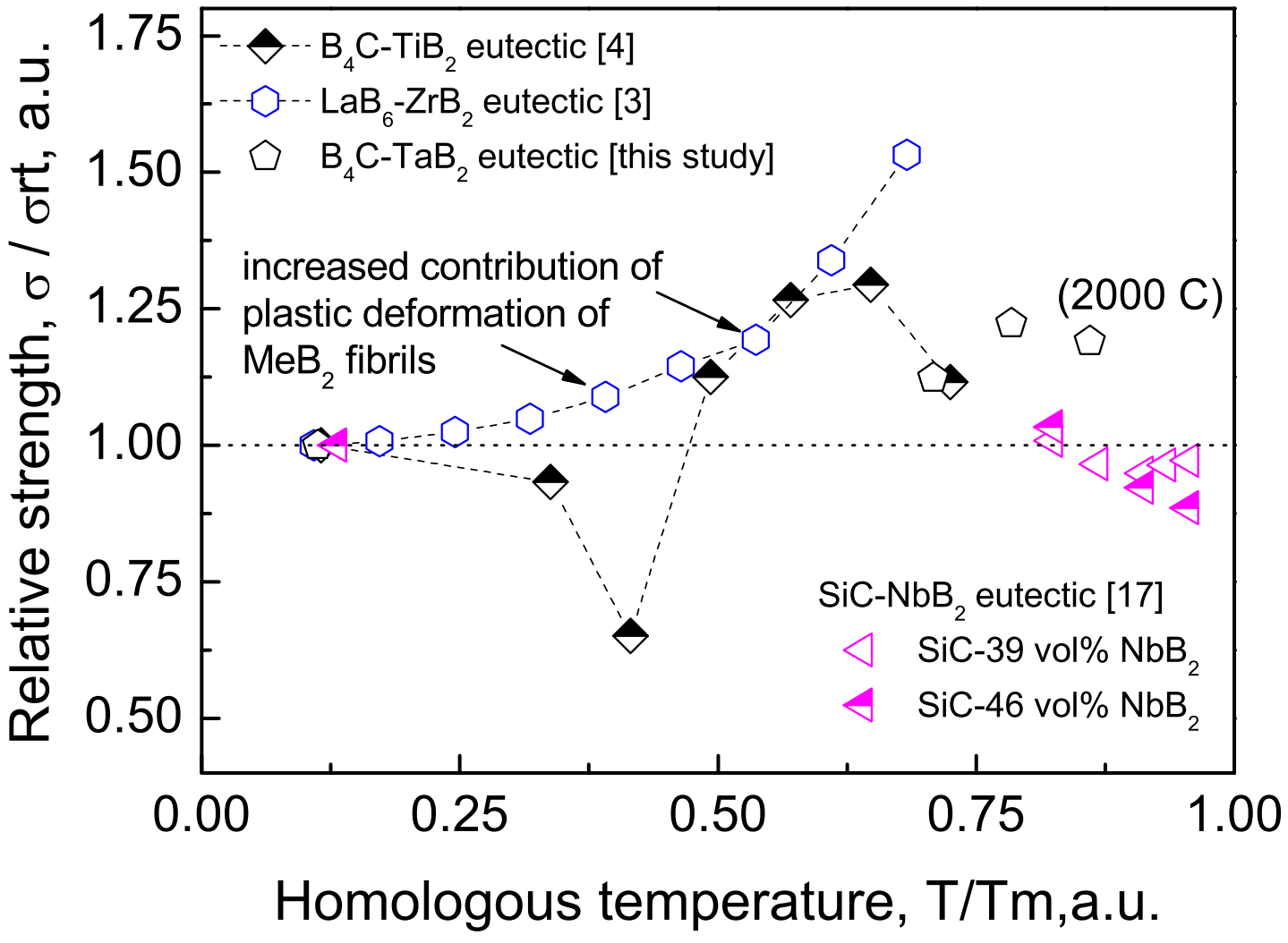
Relative strength, σ / σrt, a.u.
1.75
1.50
1.25
1.00
0.75
0.50
0.00
0.25
0.50
0.75
1.00
Homologous temperature, T/Tm,a.u.
B4C-TiB2 eutectic [4]
LaB6-ZrB2 eutectic [3]
B4C-TaB2 eutectic [this study]
increased contribution of
plastic deformation of
MeB2 fibrils
(2000 C)
SiC-NbB2 eutectic [17]
SiC-39 vol% NbB2
SiC-46 vol% NbB2